JOURNAL OF MATERIALS SCIENCE 14 (1979) 1694–1706

New glass-ceramic materials for prosthetic applications

F. PERNOT, J. ZARZYCKI
Laboratoire des Verres du C.N.R.S., Laboratoire de Science des Matériaux, Université de Montpellier II, France

F. BONNEL, P. RABISCHONG
Unité 103 de Recherches biomécaniques de l'I.N.S.E.R.M., Montpellier, France

P. BALDET
Laboratoire d'Anatomie pathologique, Centre Gui de Chauliac, Montpellier, France

New porous vitroceramic materials have been prepared by the controlled crystallization of calcium aluminophosphate foam glasses for use in prosthetic bone replacement. The technique of elaboration was developed using DTA measurements. A study was made of their principal properties: porosity, average pore diameter, interconnections between the pores and mechanical characteristics. The biological results are also briefly described.

1. Introduction

The possibility of replacing parts of a living organism with artificial substitutes has resulted in the creation of a class of "biomaterials" which are actively studied in various laboratories throughout the world. In particular, attention is centred on the preparation of polymers for bone-implants or cardio-vascular applications and of special metal alloys and ceramics for use in dental and orthopaedic surgery.

In the latter field, metals have been used for a long time but recently the particular advantages offered by ceramics have been considered, as although bone prosthesis metals have a much greater strength than the surrounding bone, the living organism reacts unfavourably towards both the metal and the cement used for fixation. This has led to various attempts to use materials which would promote a direct bond between the bone tissue and the prosthesis.

One solution consists of replacing the metal by a vitreous material or covering the metal by a thin layer of glass which reacts chemically with the surrounding tissue and secures a permanent bond with the bone. This is essentially the technique proposed by Hench and Paschall and Greenlee *et al.* in the USA [1, 2] and in parallel developed in Western Germany [3–5]. It is possible to modify the geometry of the interface to promote better adhesion. Some interesting results were obtained by imprinting on the metallic implants the texture of corals, to simulate the porosity of natural bone [6, 7].

Another solution is to use porous materials with interconnected pores which permit tissue ingrowth and thus a perfect anchoring of the prosthesis with the surrounding bone. The successful growth requires an open porosity with definite minimal values of pore sizes and interconnections. The implant may be either entirely porous or an intermediate solution is used, consisting of a porous layer deposited onto a non-porous substrate possessing higher mechanical strengths.

Attempts to use porous alumina or calcium aluminate showed that these ceramics were well tolerated and successful bone ingrowths were obtained [8–11]. Their mechanical strength, however, was rather low, which resulted in a search for materials which would be tolerated equally well by the living tissues but which possessed improved mechanical properties. This led to the idea of using glass-ceramics which are extremely

0022–2461/79/071694–13 $3.30/0

fine-grained ceramics obtained by controlled crystallization of suitable glasses and which may be tailored to possess excellent mechanical properties.

In the use of porous materials the principal handicap is their mechanical weakness due to the large size of the pores required for successful mineralized bone ingrowth. The minimum size of the interconnections between the pores should be about 100 μm and this condition is to be satisfied from the start in the case of biologically inert (non-reacting) materials, such as alumina or calcium aluminates, leading to structurally weak components unsuitable for most prosthetic applications. If however, the porous material could be made partially biodegradable (some attempts have already been made with tricalcic-phosphates [12]), the size of the interconnections between the pores could be reduced to about 15 μm in order to allow the initial ingrowth of the fibrous tissue. The subsequent widening of the passages by biodegradation could then allow the transformation of this tissue into mineralized bone. Having smaller pores, such a material would be initially stronger until the mineralized bone ingrowth would compensate for the widening of the pores by biodegradation.

This paper describes attempts to synthesize such a porous, biodegradable glass-ceramic material for use in orthopaedic surgery. The methods of elaboration and characterization of the materials will be presented; the biological results will only be summarized, their detailed description will be the subject of a separate paper [15].

2. Preparation

To obtain a glass-ceramic material, a base-glass of a suitable composition containing a proper nucleant is converted into a highly crystallized, fine-grained material by thermal treatments which involve nucleation and growth steps. If the final glass-ceramic is to be porous, it is necessary to introduce porosity into the base-glass by a method used classically to make a "foam" glass [16] and which consists of inducing a gas evolution in the viscous glass. In the method of synthesis developed here, the "foaming" and ceramization steps were realized during a single heat-treatment.

The suitable base-glass is ground to powder (granulometry less than 270 mesh). A foaming agent, i.e. a compound which gives off gas through decomposition or reaction with the glass, is added and thoroughly mixed with the glass powder. mixture is then heat-treated at a temperature above the transformation temperature, T_g, of the glass to allow the sintering of the glass particles which imprison the particles of the foaming agent. If necessary, the temperature is then increased until the foaming agent reacts. The gas evolved inside the glass mass of a low viscosity produces a foaming effect. It is only after the onset of foaming that the ceramization steps should begin. Crystallization has a two-fold function – it arrests foaming when the pores have reached a suitable size and brings about the general increase in mechanical strength of the material due to the conversion of glass into a microcrystalline phase.

In practice the method requires a careful choice of base-glass, foaming agent and thermal treatment cycle.

3. Choice of base glass

In the first instance, biological criteria are essential: the base glass should be well accepted by the living organism and, if possible, slowly biodegradable within the bone tissue. Since the mineral substance of the bone is essentially hydroxyapathite, systems based on calcium phosphates were chosen for the base glass.

In the binary system $CaO–P_2O_5$ glass formation occurs only up to 55 mol% CaO [17]; this eliminated tricalcium phosphate ceramics previously mentioned [12–14]. Studies were made essentially on glasses having the composition of calcium metaphosphate $Ca(PO_3)_2$ and various calcium alumino-phosphates.

Physical criteria governing the choice of a suitable glass composition stem from the method of synthesis briefly outlined above. The heat-treatments to which the mixture (glass + foaming agent) is submitted should be in a temperature range which promotes crystallization but sintering of the glass particles and especially the foaming should occur when the material is still sufficiently viscous. It is, therefore, necessary that the selected glass should possess a relatively small crystallization rate at the heat-treatment temperatures. This is even more imperative, as grinding glass into a powder increases its crystallization tendency by heterogeneous (surface) nucleation mechanisms. It should also be mentioned that the addition of the foaming agent ($CaCO_3$ in all studies) may bring about a similar accelerating effect. The choice of a biologically suitable base-glass having the required physical properties was made using differential thermal analysis (DTA) techniques.

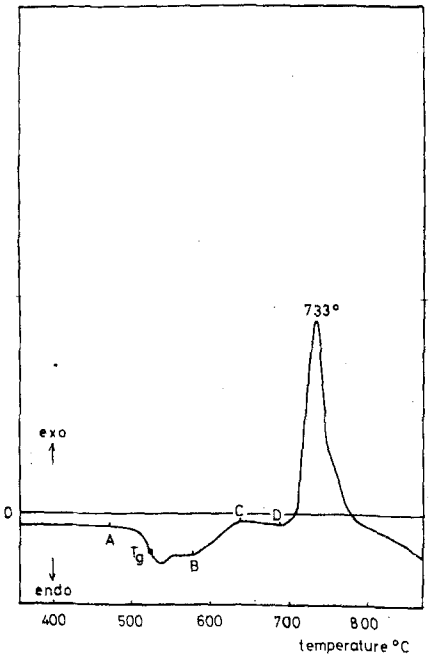

Figure 1 DTA curve of a calcium aluminium phosphate glass (80 $Ca(PO_3)_2$–20$AlPO_4$)

In the studies presented below a micro DTA analyser* was used working at low heating rates ($10^\circ C/min^{-1}$) to approximate effective isothermal elaboration conditions.

3.1. Calcium-alumino-phosphate glasses

The best results were obtained with a glass of the system P_2O_5–CaO–Al_2O_3. Its composition is chosen to fall at the intersection of the binary joins: CaO, P_2O_5–Al_2O_3, P_2O_5 and $2CaO$, P_2O_5–Al_2O_3, $3P_2O_5$ [18]. The base glass was obtained by melting a mixture of $Ca(H_2PO_4)_2$ H_2O + $AlPO_4$ in a Pt–10% Rh crucible at 1200°C. The batch was previously dehydrated at 100° C for 12 h.

The DTA curve of this glass (Fig. 1) shows an endothermal feature ABC at the beginning of which the glass transition temperature, T_g = 525° C, can be located. After return to the base line at about 630° C (point C) a pronounced exothermal peak starts; point D at 960° C corresponds to the onset of crystallization. According to Yamamoto [19] the average sintering temperature of the glass (corresponding to a viscosity of 10^6 P) is to be placed in the BC interval.

A mixture of this glass and $CaCO_3$ (foaming agent) heated for 1 h at 650° C shows evidence of sintering and foaming prior to crystallization. At this temperature, the CO_2 release is due to the glass being attacked by the carbonate, corresponding schematically to the reaction:

$$\text{glass } CaOP_2O_5 + CaCO_3 \rightarrow \text{glass } 2CaO, P_2O_5 + CO_2. \quad (1)$$

At lower temperatures this reaction no longer occurs and heating for 1 h at 600° C resulted only in sintering; additional heat-treatment for 45 min at 650° C still induced foaming. Thus sintering and reaction 1 occurred simultaneously in the first case

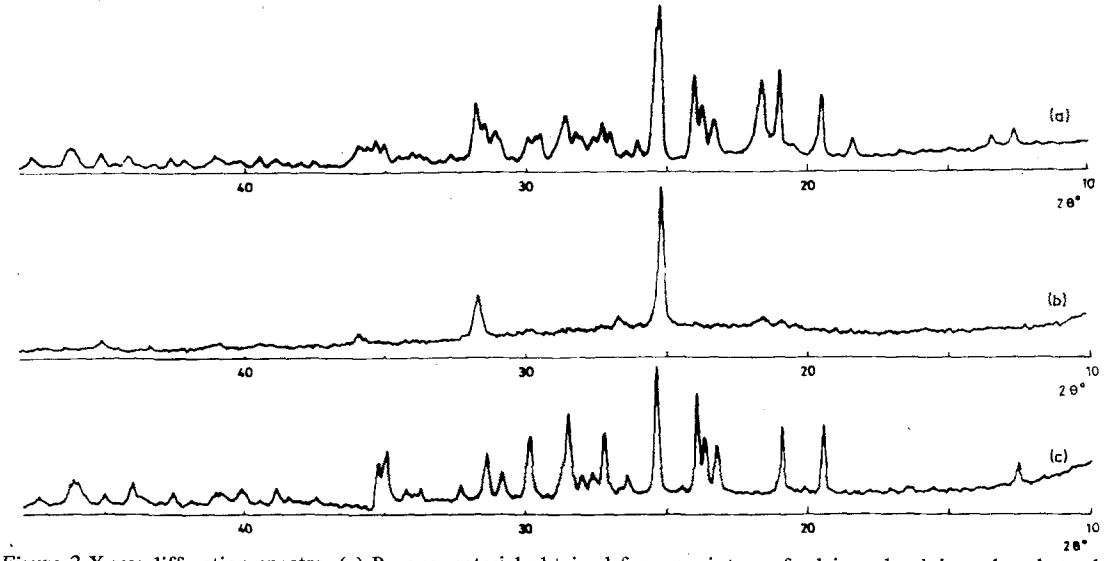

Figure 2 X-ray diffraction spectra. (a) Porous material obtained from a mixture of calcium aluminium phosphate glass and $CaCO_3$, heat-treated for 1 h at 650° C. (b) Calcium aluminium phosphate glass, without $CaCO_3$, heat-treated for 1 h at 650° C. (c) Pure calcium metaphosphate glass heat-treated for 1 h at 650° C.

*BDL – type M2.

and successively in the second case before the material crystallized to an appreciable extent.

The catalysing role of the foaming agent is evident from the X-ray diffraction spectra of the porous materials (Fig. 2a) which show that they are crystallized to a great extent. The crystalline phase corresponds to calcium metaphosphate (Fig. 2c).

The same base-glass powder heat-treated at 650°C without the foaming agent leads to compact glass with only traces of crystallization. The corresponding X-ray diffraction spectrum (Fig. 2b) shows that an important quantity of glass phase remains.

The process of crystallization of the porous material may be explained as follows: initially, before the carbonate starts reacting, the sintering of glass particles encloses $CaCO_3$ particles; Reaction 1 occurs and the crystalline phase formed promotes bulk crystallization of the glass. This makes the system more rigid and arrests foaming at a point when the pores reach the size required for biological application. The following example will make more evident the importance of the crystallization process and the precise moment when it occurs.

3.2. Calcium metaphosphate glass

This glass was similarly obtained by melting at about 1200°C monocalcium phosphate $Ca(H_2PO_4)_2$, H_2O which had been previously dehydrated at 110°C for 12 h. The DTA curve of this glass is shown in Fig. 6; contrary to the case of calcium alouminophosphate (Fig. 3a) it can be seen that the portion CD is not present, and crystallization occurs before the return to base line is achieved. This is evident in the small shoulder at 610°C preceding the important peak culminating at 657°C.

A heat-treatment indentical to the one given for the preceding batch (1 h at 650°C) leads to inadequate sintering and absence of foaming. The glass crystallizes faster than it sinters which results in cracks observable in the end product. Reaction with the foaming agent occurs once the material has become more rigid through crystallization; the higher viscosity prevents the pores from enlarging and the released CO_2 escapes through small cracks distributed throughout the material.

This fast crystallization behaviour is evident even in the absence of $CaCO_3$. Heat-treatment of pure vitreous metaphosphate powder for 1 h at 650°C results in a fully crystallized (Fig. 2c) and slightly sintered material. X-ray diffraction spectra correspond to CaP_2O_6 in agreement with the literature [20] and are identical to the previous case (Fig. 2a).

3.3. Calcium–sodium–silicate glass

The previous example corresponded to the case where crystallization occurs too rapidly. To illustrate the opposite case, when crystallization does not readily occur, industrial SiO_2, Na_2O, CaO glass may be chosen. The corresponding DTA curve is shown in Fig. 3c. The material remains viscous during the sintering and foaming stages. As no crystallization occurs to stop the bubbles growing, the final product is very light with large pores. It lacks mechanical strength and can be crushed by hand.

Systematic study has shown that of all the different glasses, calcium aluminophosphates (CAP) give the most satisfactory results; efforts were therefore centred on this type of material. Mixtures of CAP glass and $CaCO_3$ were treated in Au–5% Pt boats to provide oblong samples suitable for mechanical tests. The lack of adherence of the material to this alloy makes the retrieval of the samples straightforward.

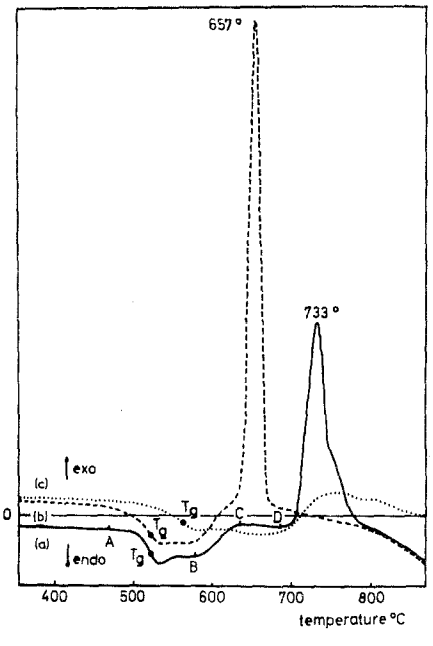

Figure 3 D.T.A. curve of some glasses which have been tested for the preparation of porous glass-ceramics. (a) Calcium aluminium phosphate glass. (b) Pure calcium metaphosphate glass. (c) sodium–calcium–silicate glass.

TABLE I Summary of the tests to obtain porous calcium aluminium phosphate glass-ceramics

CAP materials	DTA temperatures of the basic glasses (°C)				$CaCO_3$ (wt %)	Sintering and foaming temperature (°C)	Heat-treatment times (h)		
	T_g	B	C	D					
CAP 1	525	581	634	690	5	648	$1\frac{1}{2}$	(a)	(d)
2	525	581	634	690	5	650	$1\frac{1}{2}$		
3	525	581	634	690	5	650	$1\frac{1}{4}$		
4	525	581	634	690	5	650	1		
5	525	581	634	690	5	600 and 650	$1 + \frac{3}{4}$	(b)	
6	525	581	634	690	5	600 and 650	$1 + \frac{3}{4}$		
7	525	581	634	690	5	600 and 650	$1 + \frac{3}{4}$		
8	525	581	634	690	2	650	1	(c)	
9	525	581	634	690	2	650	1		
10	525	581	634	690	2	650	2		
11	525	581	634	690	2	650	2		
12	524	573	623	658	2	643	1		
13	524	573	623	658	2	646	1		
14	524	573	623	658	2	649	1		
15	524	573	623	658	1	655	1		
16	524	573	623	658	1	662	1		
17	524	573	623	658	1	677	1		
18	524	573	623	658	1	678	1		
19	524	573	623	658	1	678	1		
20	524	573	623	658	1	679	1		
21	524	573	623	658	0.5	678	1		

(a) Sintering and foaming are achieved in a single step: CAP 1 in an alumina boat, the others in a Au–5% Pt alloy boat.
(b) Heat-treatment in two steps: sintering and foaming at different temperatures.
(c) Sintering and foaming in a single step, at the same temperature.
(d) For all these materials, the pore size distribution seems rather homogeneous. They appear to be larger for CAP 1 to CAP 11 than for the others CAP 12 to CAP 21. These latter are prepared from a type-II glass which crystallizes faster than type-I glass.

Table I presents the characteristics of the various CAP materials according to the different heat-treatment schedules. Although the base-glasses were always prepared from identical batches, they do not all have the same DTA curve. Fig. 4 shows the two main types encountered. For "type II" glasses (Fig. 4b) the CD interval is smaller and the exothermal peak sharper. This results in a more rapid arrest of foaming through crystallization (CAP 12 to 25 in Table I).

The difference in crystallization rates could be due to the variation of OH content from glass one to another. It has already been shown that OH radicals influence the crystallization kinetics of calcium metaphosphate glass [21]. During the melting of batches, OH could not be evolved in the same proportions, and two facts seem to confirm the hypothesis:

(1) the lighter the weight of the batches, the higher the DTA crystallization peak temperature;

(2) this temperature is also higher when the glass is remelted.

To induce porosity changes, the proportion of the foaming agent was varied between 5 and 0.5 wt%.

In most of the materials prepared, sintering and foaming occurred at the same temperature. In the case of CAP 5, 6 and 7, these operations were carried out at different temperatures. This resulted in only slight differences in the end products.

For several CAP materials prepared from "type II" base-glasses, it proved more advantageous to shift the temperature of the heat-treatment slightly beyond point D. The corresponding increase in crystallization rate was apparently compensated by a much quicker increase of the reaction rate between the glass and $CaCO_3$.

4. Characterization of the materials

The intended use of these materials in orthopaedics imposes mechanical and biological constraints. Their porosity should suit bone tissue growth requirements. At the same time, however, they should have sufficiently high initial mech-

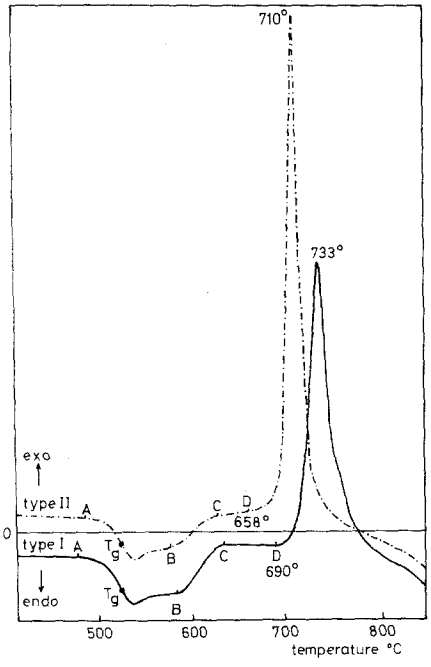

Figure 4 DTA curves of two calcium aluminium phosphate glasses, with the same composition, prepared from a mixture of $Ca(H_2PO_4)_2 \cdot H_2O$, $AlPO_4$.

anical strengths compatible with their use as bone implants. A series of physical tests was performed to characterize the texture of the materials and measure their mechanical constants to permit optimization.

4.1. Porosity tests

Most of these tests followed the directions issued by the European Federation of Refractory Manufacturers (P.R.E.) [22]. The following characteristics were measured: bulk density (pycnometric method); apparent density, open porosity (Archimedes' method); total porosity from apparent volume; fractions of total and closed porosity; pore size evaluation by scanning electron microscopy; and interconnection pore size distribution, by mercury porosimetry [8, 23]. This last technique is based on the fact that increasing pressure is needed to force mercury into smaller and smaller pores. The corresponding absolute pressure, P, required is related to the interconnection pore size, d, by the relation:

$$d = \frac{15932}{P}$$

where d is expressed in μm and P in g cm^{-2}.

A specimen of a known bulk volume is placed in a pycnometer chamber, evacuated to 10^{-3} g cm^{-2}. Mercury is then admitted and the pressure increased stepwise up to atmospheric pressure. The mercury volume admitted during each pressure increase is recorded. Interconnection pore size distribution is then obtained from a plot of the incremental volumes, V_P, of the mercury intruded versus the absolute pressure required to produce each volume increment. This method allows the measurement of the interconnection pore sizes between 450 and 15 μm. Since biological applications require minimal interconnection pore sizes of about 15 μm, it is evident that most of the pores should be filled by mercury when atmospheric pressure is reached.

The results of these tests are shown in Table II. The following remarks may be made.

(1) For heat-treatments at the same temperatures (e.g. 650° C), the total porosity decreases from 75% to 35% when the proportion of the foaming agent ($CaCO_3$) decreases from 5% to 1%.

(2) For the highest $CaCO_3$ content (5%) the porosity decreases with the length of heat-treatment (CAP 1 and 7).

(3) For up to 2% $CaCO_3$, duration of heat-treatment for more than 1 h does not seem to play any role (CAP 9 and 11).

(4) The porosity is almost entirely an open one –there is seldom a difference of more than 2% between the open and total porosity. This difference increases, however, when the porosity decreases which may be explained by the difficulties of establishing interconnection when the distribution density of bubbles gets smaller.

The interconnections between the pores may be easily observed on scanning electron micrographs (Fig. 5).

The interconnection pore size distributions are not directly related to the porosity; their maxima are situated between 70 and 15 μm (Fig. 6b and c), exceptionally the maximum is situated between 110 and 60 μm for the CAP 7 material, elaborated in two steps (Fig. 6a). On each sigmoïdal curve, an average diameter, d_m, can be defined when half of the pore volume is filled with mercury. In the present case, one can notice that $d_{m,a} > d_{m,b} > d_{m,c}$. This last result can be related to pore size evaluation made by scanning electron microscopy (Fig. 7). The pores can be considered as interconnecting spheres with diameter D, the intersection diameters of which correspond to d, previously

TABLE II Porosities of the calcium aluminium phosphate glass-ceramics

Materials	$CaCO_3$ (wt %)	Heat-treatment temperature (°C)	Heat-treatment times (h)	Absolute density	Apparent density		Porosities (%)					
					D_a	D_a^*	Open		Total		Closed	
							π_a	π_a^*	π_t	π_t^*		
CAP 1	5	648	$1\frac{1}{2}$	2.71	0.82	0.80	69	70	69,5	70.5	~0.5	Materials prepared from a type-I glass
3	5	650	$1\frac{1}{4}$	2.71	0.88	0.84	66.5	68	67,5	69	1	
7	5	600 and 650	$1+\frac{3}{4}$	2.71	0.99	0.95	62.5	64	63,5	65	1	
9	2	650	1	2.71	1.40	1.37	46	48	48	49.5	1.5–2	
11	2	650	2	2.71	1.38	1.33	47	49	49	51	2	
12	2	643	1	2.71	1.33	1.24	54	–	–	54	0	Materials prepared from a type-II glass
13	2	646	1	2.71	1.26	1.23	52.5	52.5	53.5	54.5	1–2	
14	2	649	1	2.71	1.27	1.21	52	54.5	53	55	0.5–1	
15	1	655	1	2.71	1.67	1.66	35.5	36	38	38.5	2.5	
16	1	662	1	2.71	1.66	1.61	36.5	38.5	39	40.5	2–2.5	
17	1	677	1	2.71	1.62	1.57	37.5	39	40	42	2.5–3	
18	1	678	1	2.71	1.31	1.15	49.5	53.7	52	57.5	2.5–4	
19	1	678	1	2.71	1.26	1.22	51.5	53	53.5	55	2	
20	1	679	1	2.71	1.28	1.26	51.0	53	53.5	53.5	0.5–2.5	
21	0.5	678	1	2.71	1.86	1.77	24.5	28	31	34.5	6.5	
22	5	653	1	2.71	0.65	0.59	75	77.5	76	78	0.5–1	
23	5	650	1	2.71	0.68	0.62	74.5	76.5	75	77	0.5	
24	2	679	1	2.71	1.09	1.09	58.5	58.5	59.5	59.5	1	
25	2	679	1	2.71	1.09	1.09	59	59	59.5	59.5	0.5	

*Values calculated from the apparent volume.

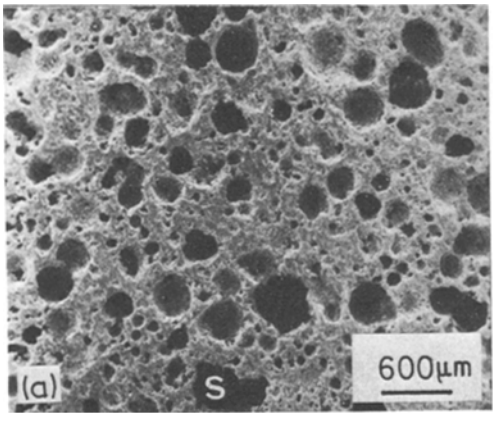

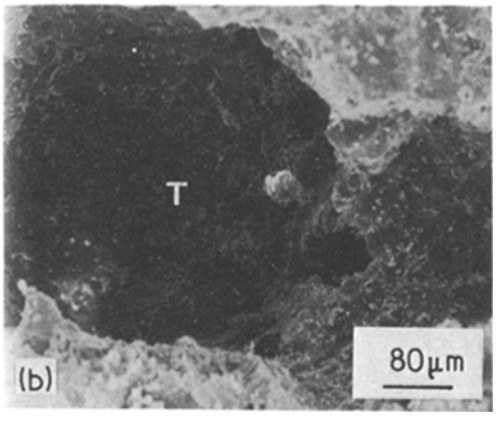

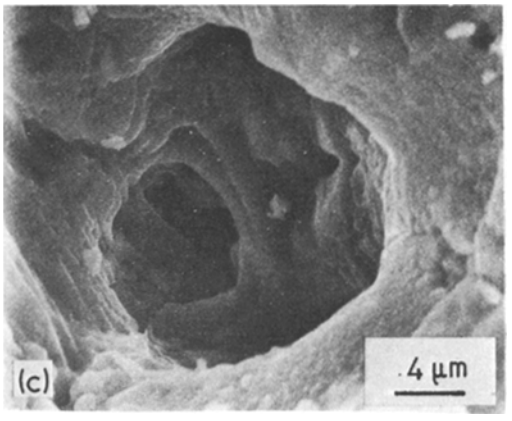

Figure 5 Scanning electron micrographs of a porous glass-ceramic (50% porosity). (a) General view of the surface. (b) More detailed view of pore S. (c) More detailed view of hole T.

measured. In a given material, with a porosity P, an average diameter D_m can be defined, the average distance of the centres being constant. These different hypotheses result in two conclusions.

(1) If, in a more porous material such as CAP 7 (65%) (Fig. 7a), pores reach a size approximately similar to CAP 9 material (50%) (Fig. 7c) ($D_{m,a} \simeq D_{m,c}$), interconnections will be of a greater size. Such an observation was made by comparing Fig. 6a and c: the interconnection diameter $d_{m,a}$ of the 65% material is greater than $d_{m,c}$ for the 50% material.

(2) In another case, some materials such as CAP 7 (Fig. 7a) may have larger pores than those of CAP 1 (Fig. 7b) ($D_{m,a} > D_{m,b}$), but their porosity is rather similar, respectively 65% and 70%. In that case the interconnection diameter d_m varies as D_m. This can be observed in Fig. 6a and b ($d_{m,a} > d_{m,b}$).

Apart from these observations which are general, one should mention differences between

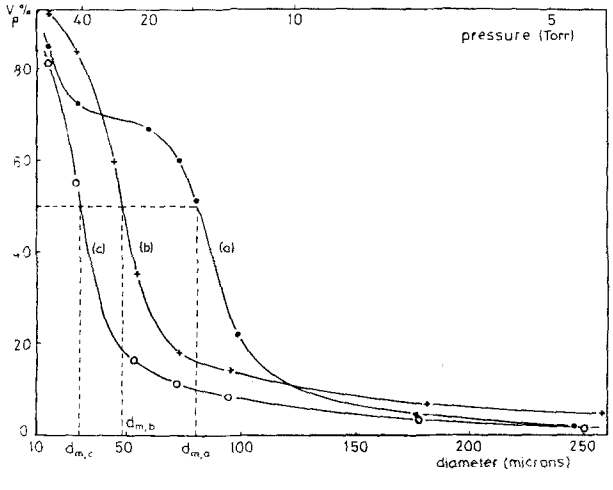

Figure 6 Interconnection pore size distribution curves, established by mercury porosimetry. Porosities of glass-ceramics studied: (a) 65%; (b) 70%; (c) 50%.

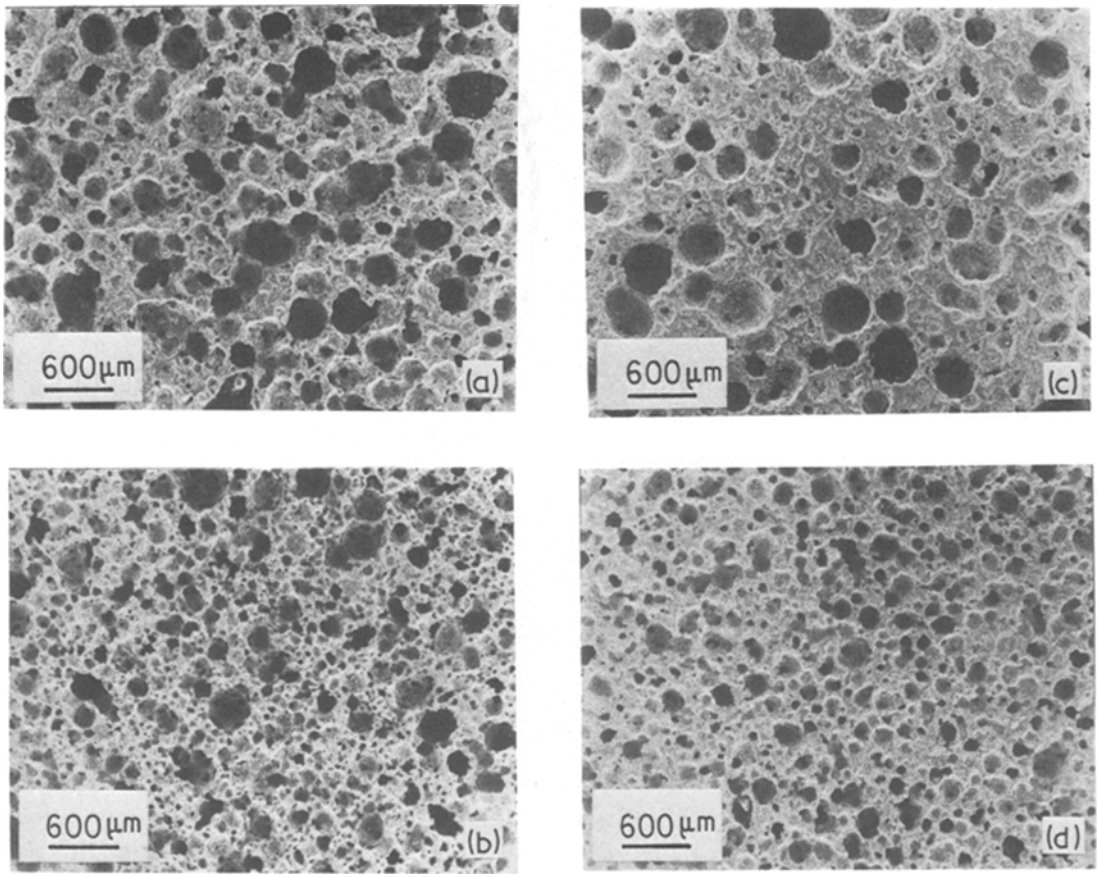

Figure 7 Scanning electron micrographs of some porous glass-ceramics; porosity of the materials: (a) 65%; (b) 70%; (c) 50%; (d) 50%.

CAP 1 to 11 materials and CAP 12 to 15, prepared from type-II glass. In the latter series, porosity size decreases with the fraction of foaming agent, but for the same quantity of $CaCO_3$ the porosity tends to be higher. These results cannot be explained merely by differences in the heat-treatment temperatures; other factors such as the glass and carbonate's granulometry should also be included.

4.2. Mechanical properties

To evaluate the mechanical properties of the materials, the fracture bending stress and Young's modulus were measured using two types of sample of approximate dimensions (in mm): (A) 80 × 10 × 5 and (B) 40 × 5 × 3. The longer samples were cut thick enough to minimize effects due to inhomogeneities of pore distribution in the fracture surface. The samples were subjected to a bending test in a four-point loading mode on an Instron machine with a cross-head speed of 0.5 mm/min^{-1} for sample (A), 0.2 mm/min^{-1} for sample (B). The load–deflection curves are not uniformly linear over the whole test interval (Fig. 8a), they are sometimes sigmoïdal (Fig. 8b), or present features found in controlled crack propagation (Fig. 8c). The experimental results are given in Table III.

4.2.1. Fracture bending stress

It can be seen that the fracture bending stress, which is about 400×10^5 Nm^{-2} for a material with 35% porosity, falls to 70×10^5 Nm^{-2} for the 75% porosity. For the sake of comparison, values were included relative to alumina of comparable porosity (Table IV); it can be seen that CAP materials compare favourably with this material. The

TABLE III Mechanical properties of porous calcium aluminium phosphate glass-ceramics

Materials	$CaCO_3$ (wt %)	Heat-treatment temperatures (°C)	Heat-treatment times (h)	Total porosity (%)	Fracture bending stress (10^5 Nm^{-2})		Young's modulus (10^7 Nm^{-2})		
					(A)	(B)	("Instron")		("Cabarat")
							(A)	(B)	(A)
CAP 2	5	650	$1\frac{1}{2}$	75	68	70	358	327	428
3	5	650	$1\frac{1}{4}$	69	93		501		
4	5	650	1	70	84	88	473	416	565
5	5	600 and 650	$1 + \frac{3}{4}$	69	96	83	509	453	
6	5	600 and 650	$1 + \frac{3}{4}$	67	93	84	570	460	664
7	5	600 and 650	$1 + \frac{3}{4}$	65	112	105	649	538	
8	2	650	1	50	227	227	1425	1185	1669
9	2	650	1	50	236	235	1494	1231	
10	2	650	2	51	224	231	1427	1365	1368
11	2	650	2	51	237	228	1470	1267	
12	2	643	1	55	200	161	1291	996	
13	2	646	1	54.5		190		1048	
14	2	649	1	55.5	194	195	1184	1010	
15	1	655	1	40	409	359	2300	1746	
16	1	662	1	42	328	284	2100	1667	
17	1	677	1	42	334	332	2174	1780	
18	1	678	1	57.5		242		1218	
19	1	678	1	55	182	216	1340	1157	
20	1	679	1	53.5		224		1045	
21	0.5	678	1	35	370	348	2480	2183	
22	5	653	1	76	45	44	315	242	
23	5	650	1	75.5	42	41	326	224	
24	2	679	1	60	170	151	965	719	
25	2	679	1	60	165	136	986	636	
Base-glass	0								6400

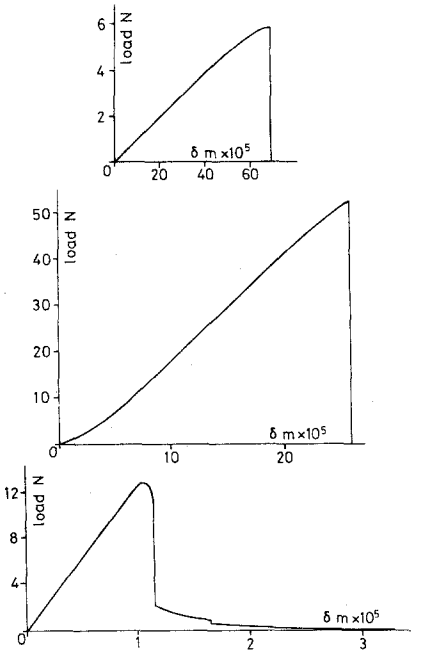

Figure 8 Load versus strain δ curve for some samples obtained with an Instron tester at 0.5 or 0.2 mm min^{-1} cross-head speed. (a) The most common aspect: a linear part followed by a slight curvature before fracture. (b) Sigmoidal aspect: curvature at the beginning and at the end, linear part in the middle. (c) Half-stable fracture (specimen B; cross-head speed: 0.2 mm min^{-1}).

difference noted for a 50% porosity material is due to alumina having a more open structure: interconnection pore size is greater than 200 μm for more than 73% pores, which for CAP is less than 100 μm for 90% pores. At equal porosity, the strongest material seem to be that with the smaller interconnection pore size.

4.2.2. Young's modulus determination

Young's modulus was obtained from the linear portion of the load–deflection curves. It depends directly on porosity (Table III). For the CAP 2, 4, 6 and 10 materials, a dynamic mode of determination using Cabarat's elasticimeter [24] was used. Young's modulus is then calculated from the resonance frequency of transverse vibrations in the kHz range. Values obtained in this way are higher than those from static measurements. This is due to the particular texture of the samples.

4.2.3. Dependence of Young's modulus on porosity

For porous materials, the dependence of Young's modulus, E, on porosity, P, is commonly fitted to

TABLE IV Comparison between fracture bending stress values relative to calcium aluminium phosphate glass-ceramics and alumina of comparable porosity

Open	Fracture bending stress ($Nm^2 \times 10^{-5}$)	
	Al_2O_3*	CAP
75	60	68
65	111	111
50	114	237

*These materials have been prepared by "Société Française de Céramique" for a contract A.T.P. 3/73/24 entitled "Les Céramiques Implantables" which took place between D.G.R.S.T. and I.N.S.E.R.M. (U 103).

an empirical relation [25] derived from a formula of the type:

$$E = E_0 \exp(-bP) \quad (2)$$

where E_0 and b are constants determined experimentally. First order developments such as:

$$E = E_0 (1 - bP) \quad (3)$$

are also used. Fig. 9 and 10 show, respectively, the application of these relationships to the results obtained in this study; results obtained for long and short specimens were plotted seperately. The simple Equation 3 is seen to be well verified for porosities between 40 and 70%. For longer specimens, deviation is less than 10%; it reaches 20% for short specimens.

Values of E_0 and b obtained from these plots are, respectively:

E_0	b
4400×10^7 Nm^{-2}	1.28
3500×10^7 Nm^{-2}	1.26

The b values are lower than those obtained for other porous materials [22] which range from 2 to 3. The E_0 values do not correspond to the Young's

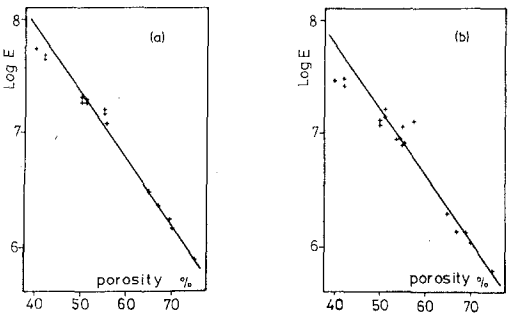

Figure 9 A plot of log E versus porosity, (a) for (A) specimens, (b) for (B) specimens.

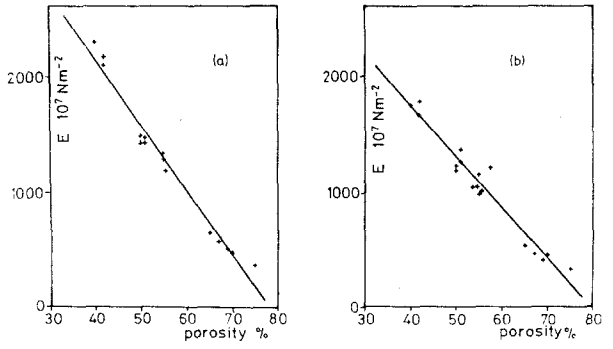

Figure 10 A plot of Young's modulus, E, versus porosity, (a) for (A) specimens, (b) for (B) specimens.

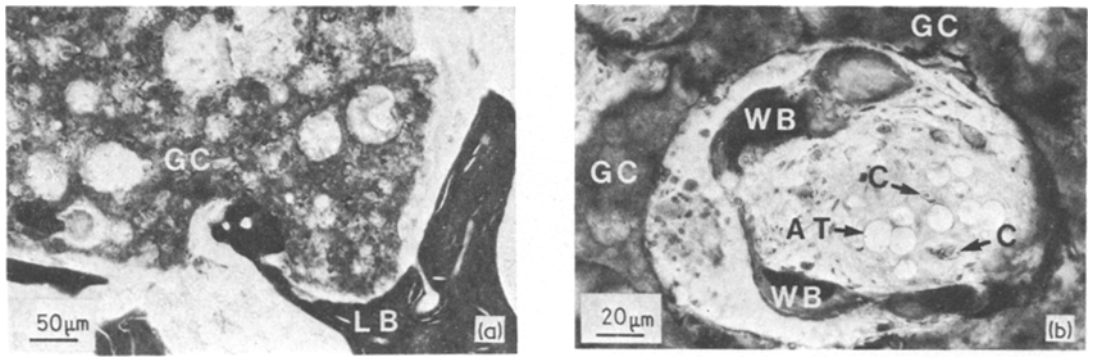

Figure 11 Observation of bone growth outside (a) and inside (b) the implants of glass-ceramics, CAP. GC glass ceramic; LB lamellar bone; WB woven bone; AT adipose tissue; C capillary

modulus of CAP material with zero porosity which is 6400×10^7 Nm^{-2}. This confirms that the linear approximation is insufficient in the whole P range. The same applies to the exponential Equation 2 which leads to much higher values of b and E_0.

5. Biological studies

Samples of porosity ranging from 50 to 70% were implanted in the greater trochanter and under the tibial plate of experimental animals (rabbits). The animals were killed after periods of 1 to 3 months; samples embedded in hard plastic were cut into slices of 0.5 to 1 mm and then ground down to 50 μm thickness. The samples were stained with Masson's trichrom and Villanueva's osteochrom.

Whatever their degree of porosity, the implants showed from the first month the beginnings of embedding in a fibrous tissue in which appear trabeculae of lamellar bone directly continuous with those of the neighbouring bone (Fig. 11a). The pores of the implants were totally invaded by a vascular-fibrous tissue in which appeared primary woven bone. This phenomenon was more pronounced after the second month.

At the third month, embedding of the implant was complete; a giant-cell reaction with resorption was noted at the periphery. The pores were totally filled by primary woven bone (Fig. 11b).

In the case of implants with 70% porosity, fracturing of the material was observed.

References

1. L. L. HENCH and H. A. PASCHALL, *J. Biomed. Mater. Res. Symposium*, 4 (1973) 25.
2. T. K. GREENLEE Jr, C. A. BECKHAM, A. R. CREBO and J. C. MALMORG, *J. Biomed. Mater. Res.* 6 (1972) 235.
3. H. BROEMER, H. H. KAES and E. PFEIL, Ernst Leitz G.m.b.H., Wetzlar, Germany, US patent no. 3 922 155, 25 November 1975.
4. V. STRUNZ, M. BUNTE, R. STELLMACH, U. M. GROSS, K. KUHL, H. BROMER and K. DEUTSCHER, *Dtsch. Zahnärztl. Z.* 32 (1977) 287.
5. M. BUNTE, V. STRUNZ, U. M. GROSS, K. KUHL, H. BROMER and K. DEUTSCHER, *ibid.* 32 (1977) 323.
6. E. W. WHITE, J. N. WEBER, D. M. ROY, E. L. OWEN, R. T. CHIROFF and R. A. WHITE, *J. Biomed. Mater. Res. Symp.* 6 (1975) 23.
7. R. T. CHIROFF, E. V. WHITE, J. N. WEBER and D. M. ROY, *J. Biomed. Mater. Res.* 9 (1975) 29.
8. J. J. KLAWITTER and S. F. HULBERT, *J. Biomed. Mater. Res. Symp.* 2 161.

9. S. LYNG, E. SUNDMAN, S. F. HULBERT and B. W. SAUER, *Acta orthop. scand.* 44 (1973) 694.
10. P. BENUM, S. LYNG, O. BO, I. RAFN and J. F. W. HAFFNER, *ibid.* 47 (1976) 158.
11. P. BENUM, S. LYNG, T. ALM and N. JOHANNESSEN, *ibid.* 48 (1977) 150.
12. G. A. GRAVES, R. L. HENTRICH, H. G. STEIN and P. K. BAJPAI, *J. Biomed. Mater. Res. Symp.* 2 (1971) 91.
13. T. D. DRISKELL, M. J. O'HARA, H. D. SHEETS Jr, G. W. GREENE, J. R. NATIELLA and J. ARMITAGE, *ibid.* 2 (1971) 345.
14. M. P. LEVIN, L. GETTER, D. E. CUTRIGHT and S. N. BHASKAR, *J. Biomed. Mater. Res.* 9 (1975) 183.
15. F. BONNEL, P. RABISCHONG, P. BALDET, F. PERNOT and J. ZARZYCKI, Journées d'études internationales sur les matériaux et implants en chirurgie ostéoarticulaire, Nancy-Vandoeuvre (1977) pp. 63–78.
16. E. O. SCHULZ, *Silikatechnik* 5 (1954) 343.
17. C. A. ELYARD, P. L. BAYNTON and H. RAWSON, *Glastech. Ber.* 32K (1959) 36.
18. P. E. STONE, E. P. EGAN Jr and J. R. LEHR, *J. Amer. Ceram. Soc.* 39 (1956) 89.
19. A. YAMAMOTO, Proceedings of the 1st International Conference on Thermal Analysis, Aberdeen, September 1965, (Macmillan, London, 1965) pp. 273–4.
20. Index (Inorganic) to the powder diffraction file (Joint Committee on Powder Diffraction Standards, 1972).
21. Y. ABE, K. MORI, A. NARUSE, Proceedings of the 18th International Congress on Glass, Vol. 14 (The Ceramic Society of Japan, Kyoto, 1974) pp. 13–19.
22. Refractory Materials; Studies and Recommendations of the "Fédération Européenne des Fabricants de Produits Réfractaires" (1972).
23. L. L. RITTER and L. G. DRAKE, *Ind. Eng. Chem.* 17 (1945) 782, 787.
24. R. CABARAT, *Verres Réfract.* 1 (1947) 26.
25. J. B. WACHTMAN Jr, "Mechanical and Thermal Properties of Ceramics," National Bureau of Standards, Special Publication 303 (1969) pp. 139–68.

Received 3 and accepted 27 November 1978.